Using Texture Analysis to Determine Human Papillomavirus Status of Oropharyngeal Squamous Cell Carcinomas on CT

K. Buch, A. Fujita, B. Li, Y. Kawashima, M.M. Qureshi, and O. Sakai

ABSTRACT

BACKGROUND AND PURPOSE: Human papillomavirus–associated oropharyngeal squamous cell carcinoma is increasing in prevalence and typically occurs in younger patients than human papillomavirus–negative squamous cell carcinoma. While imaging features of human papillomavirus–positive versus human papillomavirus–negative squamous cell carcinoma nodal metastases have been described, characteristics distinguishing human papillomavirus–positive from human papillomavirus–negative primary squamous cell carcinomas have not been well established. The purpose of this project was to evaluate the use of texture features to distinguish human papillomavirus–positive and human papillomavirus–negative primary oropharyngeal squamous cell carcinoma.

MATERIALS AND METHODS: Following institutional review board approval, 40 patients with primary oropharyngeal squamous cell carcinoma and known human papillomavirus status who underwent contrast-enhanced CT between December 2009 and October 2013 were included in this study. Segmentation of the primary lesion was manually performed with a semiautomated graphical-user interface. Following segmentation, an in-house-developed texture analysis program extracted 42 texture features from each segmented volume. A *t* test was used to evaluate differences in texture parameters between human papillomavirus–positive and human papillomavirus–negative squamous cell carcinomas.

RESULTS: Of the 40 included patients, 29 had human papillomavirus–positive oropharyngeal squamous cell carcinoma and 11 had human papillomavirus–negative oropharyngeal squamous cell carcinoma. Significant differences were seen in the histogram parameters median ($P = .006$) and entropy ($P = .016$) and squamous cell carcinoma entropy ($P = .043$).

CONCLUSIONS: There are statistically significant differences in some texture features between human papillomavirus–positive and human papillomavirus–negative oropharyngeal tumors. Texture analysis may be considered an adjunct to the evaluation of human papillomavirus status and characterization of squamous cell carcinoma.

ABBREVIATIONS: FDR = false discovery rate; GLCM = gray-level co-occurrence matrix; GLGM = gray-level gradient matrix; GLRL = gray-level run-length; HPV = human papillomavirus; SCC = squamous cell carcinoma

During the past few decades, oropharyngeal squamous cell carcinoma (SCC) has been one of the fastest growing disease sites for head and neck SCC.[1-5] Human papillomavirus (HPV) infection has been demonstrated to be an independent risk factor for the development of primary oropharyngeal SCC and may be a primary cause of the increasing incidence of oropharyngeal cancers in the United States and Europe,[2-4] in contrast to a decreasing prevalence of smoking- and alcohol-induced oropharyngeal SCCs. HPV-positive oropharyngeal SCC has also been recognized as a distinct subtype of oropharyngeal SCC.[1,3-6] Patients with HPV-positive oropharyngeal SCC are typically younger compared with patients with HPV-negative oropharyngeal SCC.[1-6] In addition to different patient demographics, HPV-positive oropharyngeal SCCs have a different prognosis and behavior pattern, including fewer secondary malignancies compared with HPV-negative oropharyngeal SCCs and an overall more favorable prognosis.[4-7]

Limited data distinguish the imaging features of primary HPV-positive oropharyngeal SCC from HPV-negative SCC.[8] Prior data describing these differences have focused on the appearance of the margins and presence of invasion into adjacent tissues.[8] In very small tumors, assessment of these proposed im-

Received September 26, 2014; accepted after revision December 28.

From the Departments of Radiology (K.B., A.F., B.L., Y.K., O.S.), Radiation Oncology (M.M.Q., O.S.), and Otolaryngology–Head and Neck Surgery (O.S.), Boston Medical Center, Boston University School of Medicine, Boston, Massachusetts.

Paper previously presented in part at: Annual Meeting of the American Society of Head and Neck Radiology, September 10–14, 2014; Seattle, Washington.

Please address correspondence to Osamu Sakai, MD, PhD, Department of Radiology, Boston Medical Center, Boston University School of Medicine, FGH Building, 3rd Floor, 820 Harrison Ave, Boston, MA 02118; e-mail: osamu.sakai@bmc.org

Indicates article with supplemental on-line table.

http://dx.doi.org/10.3174/ajnr.A4285

aging criteria can be difficult. Distinction between HPV-positive versus HPV-negative oropharyngeal SCC is important because both management and prognosis differ between these 2 groups. Prior studies have demonstrated higher response rates after induction chemotherapy and chemoradiation in addition to superior survival rates for patients with HPV-positive oropharyngeal SCCs.[7-11]

Image texture is defined as a complex visual pattern within an image consisting of simpler subpatterns with characteristic features that may be evaluated through quantitative analysis. Texture analysis is a branch of image processing that extracts texture descriptors from the image, thereby allowing the mathematic detection of subtle CT attenuation or MR imaging signal-intensity changes among image pixels. Texture analysis has been previously applied to evaluate subtle pathologic changes in an image that are not easily quantifiable by the human eye in other areas of the body, such as the liver, brain, and cartilage.[12-17]

The purpose of this study was to use texture analysis to examine differences in texture features of HPV-positive and HPV-negative oropharyngeal SCC and to see whether there are significant differences in CT texture features related to HPV-positivity.

MATERIALS AND METHODS

Following institutional review board approval, 69 patients with oropharyngeal SCC and known HPV status who underwent pretreatment contrast-enhanced CT between December 2009 and October 2013 were identified, and initial contrast-enhanced CT examinations for staging were retrospectively reviewed. Examinations with significant artifacts from motion or dental hardware were excluded. Additionally, patients with very small primary tumors (<5 mm) were also excluded. Ultimately, 40 patients were included in this study.

CT Imaging Protocol

Initial contrast-enhanced CT examinations were performed independently or in combination with FDG-PET examinations and were acquired on 64– or 16–detector row CT scanners (LightSpeed VCT or Discovery STE-16 PET/CT; GE Healthcare, Milwaukee, Wisconsin). Dedicated neck CT studies were helically acquired (120-kV/auto-mAs) at 1.25-mm intervals by using a 60-second delay after intravenous contrast injection (80–160 mL ioversol, Optiray 350; Mallinckrodt, St. Louis, Missouri; or iopamidol, Isovue 370; Bracco, Princeton, New Jersey) extending from skull base to the thoracic inlet and were reviewed in soft-tissue and bone algorithms with 2-mm thick/interval coronal and sagittal reconstructions.

Image Segmentation and Texture Analysis

The primary oropharyngeal lesion was manually contoured by a neuroradiologist with >10 years of experience in head and neck radiology and a fourth-year radiology resident, and all segmentations were validated by the neuroradiologist. Segmentation of the primary oropharyngeal lesion was performed by using a dedicated AW Workstation (GE Healthcare) with a semiautomated graphical-user interface.

Each contour was imported into in-house-developed Matlab (MathWorks, Natick, Massachusetts) texture-analysis software.

2	2	2	2
1	1	(0)	1
1	1	1	2
(0)	1	(0)	0

		Gray Level		
		0	1	2
Gray Level	0	(2)	2	0
	1	2	4	1
	2	0	1	4

FIG 1. Representation of gray-level co-occurrence matrix features. The square on the left is a representative 2-bit image. In this schematic, the gray-level co-occurrence matrix feature will count the number of times a gray level of zero occurs 2 pixels away from another gray level of zero (*black circles*). In the second row, third column, a gray level of zero (*circled in black*) is 2 pixels away from another gray level of zero in the fourth row, third column (*circled in black*). That gray level of zero in the fourth row, third column, is also 2 pixels away from a second pixel of a gray level of zero in the fourth row, first column (*circled in black*). Therefore, for this 2-bit image, the number of times a gray level of zero is within 2 pixels of another gray level of zero is 2 (*circled in black* in the Table on the right). The rest of the chart on the right is completed in a similar fashion for all other gray-level combinations by using a predefined distance of 2 pixels.

In total, 42 texture features, including 13 histogram features, 5 gray-level co-occurrence matrix (GLCM) features, 11 gray-level run-length (GLRL) features, 4 gray-level gradient matrix (GLGM) features, and 9 Law's features, were computed and averaged over the images per dataset. The histogram features calculated herein consisted of the mean, median, SD, range, geometric mean, and harmonic mean of the ROIs, which are space-invariant.[18]

In contrast to the histogram features, the GLCM features are highly spatially dependent. The GLCM is square and symmetric with rows and columns from zero to N_g, where N_g represents the number of gray tones in the image. This notation allows the GLCM element in row *i* and column *j* to represent the number of times a given gray tone of value *i* is horizontally adjacent to gray tone *j* in the original quantized image. Herein, GLCMs were calculated by using only directly adjacent pixels for simplicity. Horizontal, 45°, vertical, and 135° directions were averaged together to eliminate any directional dependence (Fig 1). We tested the following GLCM features proposed by Haralick et al[18]:

1) $$\text{Contrast} = \sum_{i,j} |i-j|^2 \, p(i,j),$$

2) $$\text{Correlation} = \sum_{i,j} \frac{(i-\mu_i)(j-\mu_j)p(i,j)}{\sigma_i \sigma_j},$$

3) $$\text{Angular Second Moment} = \sum_{i,j} p(i,j)^2,$$

4) $$\text{Homogeneity} = \sum_{i,j} \frac{p(i,j)}{1+|i-j|},$$

5) $$\text{Entropy} = \sum_{i,j} \ln[p(i,j)]p(i,j),$$

where $p(i,j)$ represents the (i,j) value of the GLCM.

In addition, the GLRL matrix provides additional insights into a spatial dependence.[18] Similar to GLCM, the GLRL matrix is quantized to N_g gray tones to simplify texture extraction and to yield a more robust technique. The row index *i* of the GLRL matrix represents the gray tone of value *i*. In contrast, the column

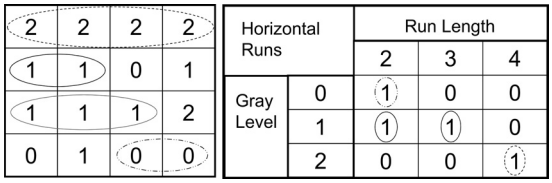

FIG 2. Representation of gray-level run-length matrix features. The square on the left is a representative 2-bit image. In this schematic, the gray-level run-length matrix will search across the image in the horizontal axis for consecutive pixels with the same gray level. In the first row of the 2-bit image, a *dotted line* circles the first row, which contains 4 consecutive pixels with a gray level of 2. In the chart on the right, this corresponds to a run length of 4 (*circled dotted line*). The second row corresponds to 2 consecutive pixels with a gray level of 1 (*black circle*), corresponding to a run length of 2 (*circled on the right chart diagram*). The third row corresponds to 3 consecutive pixels with a gray level of 1 (*gray circle*), which corresponds to a run length of 3 (*gray circle in the chart on the right*). The last column of the 2-bit image demonstrates 2 consecutive pixels with a gray level of zero (*dash-dot line*); therefore, the run length is 2 (*circled dash dot line in the chart on the right*). The calculation for gray-level run-length is also performed in the vertical axis and along a 45° axis.

index j is the run-length, which is defined as a number of adjacent and equal value pixels in a given direction. The value of each element in the GLRL matrix represents the number of pixel line segments (run) with run-length j and gray tone i (Fig 2). The same directions considered in GLCM were averaged for the GLRL matrix. The features explored included equations using short-run emphasis (SRE), long-run emphasis (LRE), gray-level nonuniformity (GLN), run-length nonuniformity (RLN), run percentage (RP), low gray-level run emphasis (LGRE), high gray-level run emphasis (HGRE), short-run low gray-level emphasis (SRLGE), short-run high gray-level emphasis (SRHGE), long-run low gray-level emphasis (LRLGE), and long-run high gray-level emphasis (LRHGE), defined as follows:

$$6)\quad \mathrm{SRE} = \frac{1}{n_r}\sum_{i,j}\frac{p(i,j)}{j^2},$$

$$7)\quad \mathrm{LRE} = \frac{1}{n_r}\sum_{i,j}p(i,j)j^2,$$

$$8)\quad \mathrm{GLN} = \frac{1}{n_r}\sum_{i}\left(\sum_{j}p(i,j)\right)^2,$$

$$9)\quad \mathrm{RLN} = \frac{1}{n_r}\sum_{j}\left(\sum_{i}p(i,j)\right)^2,$$

$$10)\quad \mathrm{RP} = \frac{n_r}{n_p},$$

$$11)\quad \mathrm{LGRE} = \frac{1}{n_r}\sum_{i,j}\frac{p(i,j)}{i^2},$$

$$12)\quad \mathrm{HGRE} = \frac{1}{n_r}\sum_{i,j}p(i,j)i^2,$$

$$13)\quad \mathrm{SRLGE} = \frac{1}{n_r}\sum_{i,j}\frac{p(i,j)}{i^2j^2},$$

$$14)\quad \mathrm{SRHGE} = \frac{1}{n_r}\sum_{i,j}\frac{p(i,j)i^2}{j^2},$$

$$15)\quad \mathrm{LRLGE} = \frac{1}{n_r}\sum_{i,j}\frac{p(i,j)j^2}{i^2},$$

$$16)\quad \mathrm{LRHGE} = \sum_{i,j}p(i,j)i^2j^2,$$

where $p(i,j)$ represents the (i,j) value of the GLRL matrix, n_r is the total number of runs, and n_p is the total number of pixels.

Finally, the GLGM was used to provide the histogram of the absolute gradient values in the ROI. As a preprocessing step, the gradient of each pixel within the ROI was computed by using a 3×3 neighborhood. The GLGM features mathematically summarize the gradient values of the pixels in the ROI and include mean, variance, skewness, and kurtosis.

Statistical Analysis

Textures features were compared between HPV-positive and HPV-negative oropharyngeal SCCs by using a Student t test for independent samples. To adjust for multiple comparisons, we performed a false discovery rate (FDR) correction and calculated the FDR-corrected P values (termed Q values) in addition to raw P values by using the method of Glickman et al[19] described in the literature. Statistical computations were performed by using SAS 9.1.3 software (SAS Institute, Cary, North Carolina). The PROC MULTTEST function in SAS was used to calculate the Q values. A 2-tailed P value $<.05$ was used to evaluate statistical significance.

RESULTS

Patient Characteristics

Twenty-nine of the 69 patients were excluded from the texture analysis. Of these 29 patients, 12 patients were excluded for artifacts generated from dental hardware and/or patient motion, 13 patients were excluded for the small size of the lesion (defined in this study as only being seen on ≤2 sections), and 4 patients were excluded because they came to our institution with only contrast-enhanced CT studies performed at another institution, which did not use our institutional imaging protocol. Ultimately, 40 patients with oropharyngeal SCC were included in this study. Patient ages ranged from 44 to 79 years of age (mean age, 62.6 ± 8.5 years) and included 33 men and 7 women.

Of the 40 patients with oropharyngeal SCC, 11 were HPV-negative (7 patients with primary sites involving the tonsil and 4 patients with primary sites involving the base of the tongue) and 29 patients were HPV-positive with primary sites involving the tonsil in 21 patients, base of the tongue in 7 patients, and soft palate in 1 patient (Fig 3). One patient of 11 with HPV-negative oropharyngeal SCC was imaged on a 64–detector row CT scanner, whereas the remaining 10 patients were imaged on a 16–detector row CT scanner. Similarly, 4 patients of 29 with HPV-positive oropharyngeal SCC were imaged on a 64–detector row CT scanner, whereas the remainder were imaged with 16–detector row CT.

Texture Analysis

The results of the texture analysis using 42 texture parameter features are given in the On-line Table. The histogram feature median demonstrated statistically significant differences between HPV-positive and HPV-negative tumors ($P = .006$). After using

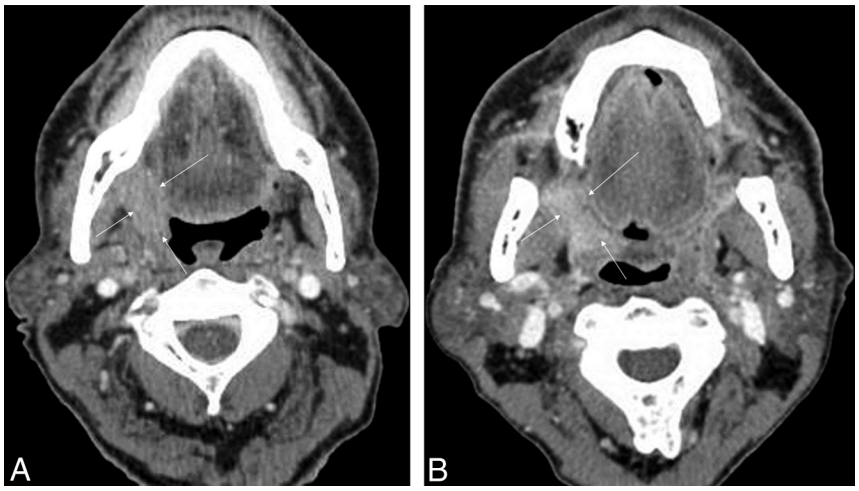

FIG 3. Representative examples of patients with HPV-positive and HPV-negative SCC. *A*, HPV-negative right tonsillar squamous cell carcinoma (*arrows*) in a 65-year-old man. *B*, HPV-positive right tonsillar squamous cell carcinoma (*arrows*) in a 65-year-old man.

the FDR correction, this difference remained statistically significant ($Q = 0.036$). The histogram feature entropy also demonstrated statistically significant differences between the 2 tumor types ($P = .016$). After we used the FDR correction, this difference remained statistically significant ($Q = 0.048$). The GLCM texture feature entropy demonstrated a statistically significant difference between HPV-positive and HPV-negative tumors ($P = .043$); however, after application of the FDR correction, this parameter was no longer statically significant ($Q = 0.21$). The remainder of the GLCM texture features and histogram features, as well as all of the GLRL features, GLGM features, and Law's features, demonstrated no statistically significant differences between HPV-positive and HPV-negative tumors.

DISCUSSION

This study demonstrated few statistically significant differences between the texture features of HPV-positive and HPV-negative primary oropharyngeal SCC. Of the 42 texture analysis features extracted from this analysis, only the histogram feature median demonstrated statistically significant differences between HPV-positive and HPV-negative oropharyngeal SCC. To date, few studies have focused on differentiating the HPV-positive and HPV-negative status of oropharyngeal SCC on CT. Cantrell et al[8] performed a blinded analysis examining CT differences of HPV-positive and HPV-negative oropharyngeal SCC and found that HPV-negative primary tumors demonstrated ill-defined borders and an increased prevalence of invasion into adjacent muscle tissue, whereas HPV-positive primary tumors tended to have well-defined borders.[8]

This paucity of studies focused on the primary site is in contradistinction to abundant literature differentiating HPV-positive from HPV-negative nodal metastasis.[20,21] For example, Goldenberg et al[20] performed a retrospective review of the pretreatment CT examinations of oropharyngeal SCC and found an increased association of cystic nodal metastases with HPV-positive base of tongue and tonsillar cancers compared with HPV-negative oropharyngeal SCCs. Well-described features of these cystic nodal metastases include a homogeneous fluid content without internal complex, irregular or solid areas, and an enhancing capsule <2 mm in thickness, whereas necrotic nodal metastases were defined as having thicker or more irregular walls with complex central low attenuation.[13] Using these imaging criteria of nodal metastasis to predict HPV status of the primary tumors revealed an 87% sensitivity when intranodal cystic changes were used as a radiologic parameter to predict HPV positivity.[6]

The distinction of HPV status of oropharyngeal SCC is clinically important because treatment and prognosis are different. Based on histopathologic studies, HPV-positive oropharyngeal SCCs are a distinctly different histologic entity compared with HPV-negative oropharyngeal SCC.[20,21] HPV-positive tumors have been described as exhibiting a basaloid, lymphoepithelial, and poorly differentiated histology compared with a keratinizing histopathology seen in HPV-negative SCCs.[7,9,22] Prior studies have described unique histologic features in nonkeratinizing HPV-positive SCCs, such as nest formation with trabeculae, pushing borders, and lack of a stromal response.[7,9,22] Furthermore, frequent mitotic features, comedonecrosis, and the presence of spindle-shaped hyperchromatic nuclei without prominent nucleoli have been described in these HPV-positive tumors.[7,9] In contrast, HPV-negative SCCs demonstrate keratinizing histopathologic features with polygonal cells with mature cytoplasm, distinct cell borders, and intercellular bridges.[7,9] The growth pattern of HPV-negative SCCs exhibits an infiltrative pattern with a pronounced stromal desmoplastic reaction not appreciated in the HPV-positive tumors.[7,9,22]

Texture analysis is a branch of image processing that seeks to reduce image information by extracting texture descriptors from the image that may allow the mathematic detection of subtle signal changes among image pixels. These techniques ultimately provide a quantitative means of extracting image features that is useful for comparative analyses. Texture analysis has been previously used to evaluate subtle pathologic changes that are not easily quantifiable by the human eye and can be particularly important in relatively normal-appearing tissues where there is subtle microscopic disruption due to early disease. Beyond the head and neck, texture analysis techniques similar to those used in this study have also been applied to myriad other organs, including the central nervous system, bone, and cartilage, among others.[12,17,23-25]

Each texture feature evaluates alternating pixel intensities according to a mathematic algorithm. The gray-level run-length features are spatially dependent texture features, and the matrices used to compute the GLRL features are based on the length and quantity of runs (adjacent pixels with similar intensity values, as explained in the "Image Segmentation and Texture Analysis" section). The short-run emphasis feature identifies whether the image has a majority of short runs, while the long-run emphasis feature identifies a majority of long runs. The gray-level nonuniformity returns a higher value if there are more gray tones with

many runs, while run-length nonuniformity returns a higher values if there are more runs with many gray tones. Run percentage is simply the normalized quantity of runs of an image, while low gray-level run emphasis and high gray-level run emphasis assess the quantity of runs from low gray-tone levels and high gray-tone levels, respectively. The short-run low gray-level emphasis, short-run high gray-level emphasis, long-run low gray-level emphasis, and long-run high gray-level emphasis are derived by combining short-run emphasis, long-run emphasis, low gray-level run emphasis, and high gray-level run emphasis. None of these features were found to have statistically significant differences between HPV-positive and HPV-negative tumors. The lack of a significant difference in these texture features between HPV-positive and HPV-negative tumors suggests a certain degree of uniformity within the tumors along both long and short matrix runs and suggests that the attenuation of both dark and bright line-like structures within the CT images is invariant of HPV tumor status.

The spatially dependent GLCM features capture the frequency of co-occurring gray tones.[18] Contrast and homogeneity are both GLCM features that represent the amount of local variation in an image; for example, high contrast and low homogeneity correspond to a finer texture with the correlation features observing streaks of similar gray-tone levels. Angular fourth moment is the fourth power of the energy of GLCM, which emphasizes a larger number of similar pixel pairs in the image. The lack of a statistically significant difference in these texture features between the 2 tumor types suggests that the level of detail of the CT images is not capable of distinguishing the 2 tumor types. The GLCM feature entropy demonstrated statistically significant differences between the 2 tumor types; however, this texture feature did not remain statistically significant after the FDR analysis. This parameter identifies the randomness and complexity of an image with higher entropy, signifying that the frequency with which 2 gray-tone values touch each other is low.[18] We believe that the significant difference in the entropy of HPV-positive and HPV-negative tumors suggests that the internal consistence of these 2 tumor types is different, despite the lack of significance on the FDR analysis.

This study has several limitations. First, there is no direct comparison between the underlying tumor histopathology and correlation to the mathematic significance of the features of a texture analysis. Ultimately, while we have postulated as to the underlying meaning in terms of the tissue architecture on the basis of the mathematic parameters of the texture analysis in cases of HPV-tumor status, it is unknown what this translates to on a histopathologic level because we have no histopathologic correlation with the results of our texture analysis. Prior studies in the literature have explored the use of a texture analysis with underlying pathology such as hepatic fibrosis in liver models, with high correlations between texture features and the degree of hepatic fibrosis; however, no direct comparison between specific texture features and histopathologic features has been performed. Second, the sample size is relatively small, totaling 40 patients. We examined only primary oropharyngeal SCCs and did not expand our cohort to include additional primary sites within the head and neck. We chose to start with primary oropharyngeal SCC because HPV-positivity is a known prognostic factor for oropharyngeal SCC.[7,8,14] Despite our small sample size, many patients had to be eliminated from the study before we performed the texture analysis, predominately due to a combination of dental artifacts, patient motion, and small lesion size. The effects of the metallic streak artifacts and patient motion on the texture analysis are not fully known or described; therefore, for this initial pilot study, we tried to collect subjects with SCCs without metallic streak artifacts, to limit this as a potential confounder.

We set a rough threshold for the lesion size, in that it would need to be seen on at least 3 CT sections to perform a good manual contour. Last, we contoured areas of obvious necrotic and cystic changes as well as ulceration of the final contours that were imported into the texture analysis program. Both HPV-positive and HPV-negative tumors demonstrated these areas of necrosis and ulceration. We eliminated these areas because including foci of air would not accurately reflect the underlying texture features within the solid portion of the tumors. Additionally, for the purposes of this initial study, we wanted to focus on whether the texture analysis could differentiate HPV status on the basis of the solid portion of the tumors.

CONCLUSIONS

The results of this pilot study demonstrate that some texture analysis features, particularly the histogram feature median, demonstrated statistically significant differences between HPV-positive and HPV-negative oropharyngeal SCCs. This study adds to the limited previously published data and suggests a potentially novel image-based assessment of HPV status of oropharyngeal SCCs on CT. The results of this study demonstrate that the quantitative, noninvasive, postprocessing assessment of a texture analysis has the potential to be used as an adjunct for the evaluation of initial oropharyngeal SCCs on CT, but further investigation into this methodology is warranted.

Disclosures: Osamu Sakai—*UNRELATED: Payment for Lectures (including service on Speakers Bureaus)*: Bracco, Kyorin USA, Eisai, *Comments*: honoraria for lecture; *Royalties*: McGraw-Hill.

REFERENCES

1. Chaturvedi AK. **Epidemiology and clinical aspects of HPV in head and neck cancers.** *Head Neck Pathol* 2012;(6 suppl 1):S16–24
2. Näsman A, Attner P, Hammarstedt L, et al. **Incidence of human papillomavirus (HPV) positive tonsillar carcinoma in Stockholm, Sweden: an epidemic of viral-induced carcinoma?** *Int J Cancer* 2009;125:362–66
3. Panwar A, Batra R, Lydiatt WM, et al. **Human papilloma virus positive oropharyngeal squamous cell carcinoma: a growing epidemic.** *Cancer Treat Rev* 2014;40:215–19
4. Pytynia KB, Dahlstrom KR, Sturgis EM. **Epidemiology of HPV-associated oropharyngeal cancer.** *Oral Oncol* 2014;50:380–86
5. Westra WH. **The changing face of head and neck cancer in the 21st century: the impact of HPV on the epidemiology and pathology of oral cancer.** *Head Neck Pathol* 2009;3:78–81
6. D'Souza G, Kreimer AR, Viscidi Ret al. **Case-control study of human papillomavirus and oropharyngeal cancer.** *N Engl J Med* 2007;356:1944–56
7. Ang KK, Harris J, Wheeler R, et al. **Human papillomavirus and survival of patients with oropharyngeal cancer.** *N Engl J Med* 2010;363:24–35
8. Cantrell SC, Peck BW, Li G, et al. **Differences in imaging characteristics of HPV-positive and HPV-negative oropharyngeal cancers: a blinded matched-pair analysis.** *AJNR Am J Neuroradiol* 2013;34:2005–09

9. Fakhry C, Westra WH, Li S, et al. **Improved survival of patients with human papillomavirus-positive head and neck squamous cell carcinoma in a prospective clinical trial.** *J Natl Cancer Inst* 2008;100:261–69
10. Kumar B, Cordell KG, Lee JS, et al. **Response to therapy and outcomes in oropharyngeal cancer are associated with biomarkers including human papillomavirus, epidermal growth factor receptor, gender, and smoking.** *Int J Radiat Oncol Biol Phys* 2007;69:S109–11
11. Weinberger PM, Yu Z, Haffty BG, et al. **Molecular classification identifies a subset of human papillomavirus–associated oropharyngeal cancers with favorable prognosis.** *J Clin Oncol* 2006;24:736–47
12. de Carvalho Alegro M, Valotta Silva A, Yumi Bando S, et al. **Texture analysis of high resolution MRI allows discrimination between febrile and afebrile initial precipitating injury in mesial temporal sclerosis.** *Magn Reson Med* 2012;68:1647–53
13. Mayerhoefer ME, Stelzeneder D, Bachbauer W, et al. **Quantitative analysis of lumbar intervertebral disc abnormalities at 3.0 Tesla: value of T(2) texture features and geometric parameters.** *NMR Biomed* 2012;25:866–72
14. Risse F, Pesic J, Young S, et al. **A texture analysis approach to quantify ventilation changes in hyperpolarised ^{3}He MRI of the rat lung in an asthma model.** *NMR Biomed* 2012;25:131–41
15. Fujimoto K, Tonan T, Azuma S, et al. **Evaluation of the mean and entropy of apparent diffusion coefficient values in chronic hepatitis C: correlation with pathologic fibrosis stage and inflammatory activity grade.** *Radiology* 2011;258:739–48
16. Jirák D, Dezortová M, Taimr P, et al. **Texture analysis of human liver.** *J Magn Reson Imaging* 2002;15:68–74
17. Anderson SW, Jara H, Ozonoff A, et al. **Effect of disease progression on liver apparent diffusion coefficient and T2 values in a murine model of hepatic fibrosis at 11.7 Tesla MRI.** *J Magn Reson Imaging* 2012;35:140–46
18. Haralick R, Shanmugam K, Dinstein I. **Textural features for image classification.** *IEEE Transactions on Systems, Man and Cybernetics* 1973;SMC-3:610–21
19. Glickman ME, Rao SR, Schultz M. **False discovery rate control is a recommended alternative to Bonferroni-type adjustments in health studies.** *J Clin Epidemiol* 2014;67:850–57
20. Goldenberg D, Begum S, Westra WH, et al. **Cystic lymph node metastasis in patients with head and neck cancer: an HPV-associated phenomenon.** *Head Neck* 2008;30:898–903
21. Marur S, D'Souza G, Westra WH, et al. **HPV-associated head and neck cancer: a virus-related cancer epidemic.** *Lancet Oncol* 2010;11:781–89
22. El-Mofty SK, Zhang MQ, Davila RM. **Histologic identification of human papillomavirus (HPV)-related squamous cell carcinoma in cervical lymph nodes: a reliable predictor of the site of an occult head and neck primary carcinoma.** *Head Neck Pathol* 2008;2:163–68
23. de Oliveira MS, D'Abreu A, França MC Jr, et al. **MRI-texture analysis of corpus callosum, thalamus, putamen, and caudate in Machado-Joseph disease.** *J Neuroimaging* 2012;22:46–52
24. Tozer DJ, Marongiu G, Swanton JK, et al. **Texture analysis of magnetization transfer maps from patients with clinically isolated syndrome and multiple sclerosis.** *J Magn Reson Imaging* 2009;30:506–13
25. Joseph GB, Baum T, Carballido-Gamio J, et al. **Texture analysis of cartilage T2 maps: individuals with risk factors for OA have higher and more heterogeneous knee cartilage MR T2 compared to normal controls— data from the osteoarthritis initiative.** *Arthritis Res Ther* 2011;13:R153